The E_p Evolutionary Slope within the Decay Phase of "FRED" Gamma-ray Burst Pulses

Z. Y. Peng [1], L. Ma [1,*], X. H. Zhao [2], Y. Yin[1], L. M. Fang[3], Y. Y. Bao[4]

ABSTRACT

Employing two samples containing of 56 and 59 well-separated FRED (fast rise and exponential decay) gamma-ray burst (GRB) pulses whose spectra are fitted by the Band spectrum and Compton model, respectively, we have investigated the evolutionary slope of E_p (where E_p is the peak energy in the $\nu F\nu$ spectrum) with time during the pulse decay phase. The bursts in the samples were observed by the Burst and Transient Source Experiment (BATSE) on the Compton Gamma-Ray Observatory. We first test the E_p evolutionary slope during the pulse decay phase predicted by Lu et al. (2007) based on the model of highly symmetric expanding fireballs in which the curvature effect of the expanding fireball surface is the key factor concerned. It is found that the evolutionary slopes are normally distributed for both samples and concentrated around the values of 0.73 and 0.76 for Band and Compton model, respectively, which is in good agreement with the theoretical expectation of Lu et al. (2007). However, the inconsistence with their results is that the intrinsic spectra of most of bursts may bear the Comptonized or thermal synchrotron spectrum, rather than the Band spectrum. The relationships between the evolutionary slope and the spectral parameters are also checked. We show the slope is correlated with E_p of time-integrated spectra as well as the photon flux but anticorrelated with the lower energy index α. In addition, a correlation between the slope and the intrinsic E_p derived by using the pseudo-redshift is also identified. The mechanisms of these correlations are unclear currently and the theoretical interpretations are required.

Subject headings: gamma rays: bursts — method: statistical

[1]Department of Physics, Yunnan Normal University, Kunming 650092, China; pzy@ynao.ac.cn

[*]Corresponding author, astromali@126.com

[2]Department of Astronomy, Nanjing University, Nanjing, Jiangsu 210093, China

[3]Department of Physics, Guangdong Institute of Education, Guangzhou 510303, China

[4]Department of Physics, Yuxi Normal College, Yuxi 653100, China

1. INTRODUCTION

The origin of the gamma-ray burst (GRB) still remains unclear though it has been found for more than forty years and many progresses have been made. The best probe of early phase of jet attributes and the physical mechanism is the prompt emission, essentially the temporal-spectral dependence of GRB pulses due to the absence of some other ways to detect them, such as gravitational wave and neutrino detections. The analysis of the GRB prompt emission provides us valuable clues to the environment from which the radiation emits and the underlying processes giving rise to the phenomenon. The spectral evolution is universal and has been studied both over the entire burst, giving the overall behavior and over individual pulse structures (see, for instance, the review by Ryde 1999). Pulses are common features in a GRB light curve and appear to be the fundamental constituent of it (see, e.g., Norris et al. 1996; Stern & Svensson 1996). This single pulse temporal evolution is often been described by a fast rise and exponential decay (the so-called FRED shape, see Fishman et al. 1994). The spectral hardness decreases during pulse decay and there are two empirical relations between the temporal and spectral properties to characterize the spectral evolution. One important correlation is that between hardness of the spectrum, the peak energy, and fluence (HFC; Liang & Kargatis 1996). The other correlation is that between hardness and the instantaneous flux (or intensity) (HIC; Golenetskii et al. 1983). The two relations appear to be satisfied by a substantial fraction of GRB pulses during the decay phase (see, Crider & Liang 1999; Ryde & Svensson 2000). Most studies concerning these correlations examine them in single pulses and do not compare the behavior of pulses within a burst. Combining the two correlations, i.e., the HIC and HFC, Ryde & Svensson (2000) showed that a power-law HIC and an exponential HFC resulted in the decay phase of the pulse following power-law behaviors described by equations 3 and 4 in their paper. Ryde & Svensson (2002) studied a sample containing 25 pulses and found that a power law gives a better description of the pulse decays than a stretched exponential, the most commonly assumed pulse shape so far. They also found that there are no obviously preferred values of the power-law index of peak energy, E_p, in the decay phase of pulse.

Daigne & Mochkovitch (2003) presented a simple, semi-analytical model to interpret the GRB temporal and spectral properties in the context of the internal shock model. The spectral evolution of synthetic pulses was first obtained with standard equipartition assumptions to estimate the post-shock magnetic field and the electron Lorentz factor. They found that $E_p \propto t^{-\delta}$, which shows the decay of peak energy during the pulses decay phase follows the power law relation with time. They also compared the consistence of the power-law index, δ, of their model with the observed index provided by Ryde & Svensson (2002) and found that the synchrotron process with standard equipartition assumptions gives a much too steep spectral evolution, which showed that another process different from synchrotron

one might radiate that energy.

The observed GRB pulses are believed to be produced in a relativistically expanding and collimated fireball because of the large energies and the short time-scales involved. The so-called Doppler effect (or curvature effect in some paper), which over the whole fireball surface would play an important role to account for the observed pulses and spectra of not only prompt GRBs but the early X-ray afterglow, is that the photons emitted from the regions on the line of sight and off the line of sight are Doppler-boosted by different factors and travel different distances before reaching the observer (e.g. Meszaros and Rees 1998; Hailey et al. 1999; Qin 2002, Qin et al. 2004, Qin 2008a, 2008b, 2008c). The curvature effect model of a cutoff power law spectrum has also been used to model the light curve and spectral evolution of the X-ray tail (Zhang et al. 2009). Based on the model of Doppler effect Lu et al. (2007) (hereafter Paper I) investigated the evolution of observed spectral peak energy E_p and found that the evolutionary curve of E_p undergoes a drop-to-rise-to-decay phase. The decay phase of the pulse, where the Doppler effect dominates, always decreases monotonically and does not necessarily reflect the corresponding intrinsic spectral evolution. They first explored the case the intrinsic spectrum is the Band function (Band et al. 1993) for three different local pulses. The three decay phases of E_p within the decay phase of the light curve were extracted and performed a linear least-squares fit to the E_p and relative observed time, τ, and have $\log E_p = I - S \log \tau$, with the same slope of $S = 0.95 \pm 0.01$ for the three curves, which indicated that the slope of the decay phase of E_p is not affected by the shape of its local pulse. Then they studied the case of intrinsic Comptonized and thermal synchrotron spectrum and found that corresponding slope $S = 0.75 \pm 0.01$ for both of the two intrinsic spectra, which also showed that the slope is independent of the forms of local pulse.

Although several GRB missions such as HETE-2 and Swift have been launched, the Burst and Transient Source Experiment (BATSE; Fishman et al. 1989), aboard the Compton Gamma Ray Observatory (CGRO; Gehrels et al. 1994), provided the largest GRB database from a single experiment among all the gamma-ray experiments that have detected GRBs. The BATSE data are still the most suitable for detailed spectral studies of GRB prompt emission, both in quantity and quality. For many of the BATSE GRBs, high time and energy resolution data are available. BATSE also provided wider energy coverage than current GRB missions.

In the present work, we select two samples observed by BATSE to investigate the evolutionary slope of E_p during the decay phase of GRB pulses. Different from what Ryde & Svensson (2002) did, we adopt those well-separated FRED pulses compiled by Peng et al. (2007). First of all, we check whether the observed evolutionary slope of E_p during the pulse

decay phase is consistent with the theoretical predication of Paper I. Examining whether the slope of E_p during the decay phase of pulse is related to other parameters such as E_p of time-integrated spectra is another motivation of this work. In section 2, we present the sample description and spectral modeling. The results are given in section 3. Discussion and conclusions are presented in the last section.

2. SAMPLE DESCRIPTION AND SPECTRAL MODELING

In this work we only select the GRB sample compiled by Peng et al. (2007) consisting of two samples provided by Kocevski et al. (2003) and Norris et al. (1999), in which the bursts are found to contain individual FRED pulses. The data with durations longer than 2 s are provided by the BATSE's LADs instruments on board the CGRO spacecraft, which provide discriminator rate with 64 ms resolution from 2.048 s before the burst to several minutes after the trigger (Fishman et al. 1994) (for more details of the sample selection, see Kocevski et al. 2003. and Norris et al. 1999). In order to obtain the evolutionary slope of E_p during the pulse decay phase (we use the symbol S to denote the evolutionary slope of E_p during the pulse decay phase) we must study the time-resolved spectroscopy. The time-resolved spectral analysis requires data with a high enough signal-to-noise (S/N) ratio to obtain better statistical results. Similar to Ryde & Svensson (2002) and Firmani et al. (2008) we also choose those bursts whose peak flux, F_p, above 1.8 photons $cm^{-2}s^{-1}$ on a 256 ms timescale to ensure a reasonable determination of the spectral parameters. In this way 78 pulses meet the criteria.

Before performing the spectral modeling we must select the type of detector, data type, and time and energy interval. Following the Kaneko et al. (2006) (hereafter Paper II) we also only use the LAD data mainly to take advantage of its larger effective area. Three LAD data types used in this work are Medium Energy Resolution data (MER), High Energy Resolution Burst data (HERB), and Continuous data (CONT) (for more detailed description about the characteristics of each data type one can refer to Paper II). To perform detailed time-resolved spectroscopy it has been shown by Preece et al. (1998) that a S/N $\sim$45 is needed. However, a high S/N will lead to time-resolved spectra consisting of only a few broader time bins. Our present work focus on the analysis of the S. Therefore the aim of our spectral analysis, of every time bin, is mainly to determine the E_p and allowing a deconvolution of the count spectrum to find the energy spectrum. In order to arrive at reliable results we need as many time bins as possible to study the S. For this purpose, we adopt the criterion that the decay phase of the pulses should have at least five time bins with $S/N \geq 30$ to be included in the study. We check that the results are consistent with higher S/N ratios. This gives us the

possibility to study the burst pulses with higher time resolution, especially for the later time bins, which is of great importance for our study.

Similar to Paper II we also use the spectral analysis software RMFIT, which was specifically developed for burst data analysis by the BATSE team (Mallozzi et al. 2005). It incorporates a fitting algorithm MFIT that employs the forwardfolding method (Briggs 1996), and the goodness of fit is determined by χ^2 minimization. One advantage of MFIT is that it utilizes model variances instead of data variances, which enables more accurate fitting even for low-count data (Ford et al. 1995).

We analyze both time-resolved and time-integrated spectra for each pulse of our sample. In addition, the entire pulse must be included in our analysis since these pulses are well-separated. The time-resolved and time-integrated spectra are modeled with two photon models. One is the most used so-called Band function (Band et al. 1993):

$$f_{BAND} = A \begin{cases} (\frac{E}{100})^{\alpha} \exp(-\frac{E(2+\alpha)}{E_{peak}}) & E < E_c, \\ (\frac{(\alpha-\beta)E_{peak}}{100(2+\alpha)})^{\alpha-\beta} \exp(\beta-\alpha)(-\frac{E}{100})^{\beta} & E \geq E_c, \end{cases} \quad (1)$$

where, $E_c = (\alpha-\beta)\frac{E_{peak}}{2+\alpha} \equiv (\alpha-\beta)E_0$. The model consists of four parameters: the amplitude A in photons s^{-1} cm^{-2} keV^{-1}, a low-energy spectral index α, a high energy spectral index β, and a νF_ν peak energy E_{peak} in keV, which is related to the e-folding energy, E_0.

Paper II have showed that the Comptonized Model (COMP model) tends to be preferable in fitting time-resolved spectra due to better χ^2 values compared with that of BAND model. Additionally, many BATSE GRB spectra lack high-energy photons (Pendleton et al. 1997). Those no-high-energy spectra are usually fitted well with this model. This also shows the existence of a number of spectra without high-energy component. Therefore, the spectra are also modeled with the COMP model. It is a low-energy power law with an exponential high-energy cutoff, which is equivalent to the BAND model without a high-energy power law, namely $\beta \rightarrow \infty$, and has the form

$$f_{COMP}(E) = A(\frac{E}{E_{piv}})^{\alpha} \exp(-\frac{E(2+\alpha)}{E_{peak}}), \quad (2)$$

E_{piv} was always fixed at 100 keV , therefore, the model consists of three parameters: A, α, and E_{peak}.

We always chose the data taken with the detector that was closest to the line of sight to the location of the GRB, as it has the strongest signal. For the case of weaker bursts the MER data is preferable because it has much finer time resolution. Whereas for the bright bursts the HERB data is preferable due to its higher energy resolution. A background estimate is made using the High Energy Resolution data (HER) data for the HERB data, covering

several thousand seconds before the trigger and after the HERB accumulation is finished. In the MER data, the CONT data are used as background. The light curve of the background, during the outburst, is modeled with a second- or third-order polynomial fit. The usable energy range for spectral analysis is $\sim$ 30 keV - $\sim$ 2 MeV for all the bursts. The lowest seven channels of HERB and two channels of MER and CONT are usually below the electronic lower energy cutoff and are excluded. The highest few channels of HERB and normally the very highest channel of MER and CONT are unbounded energy overflow channels and also not usable (see, Paper II). The procedures give us all the spectral parameters modeled by BAND and COMP model for every time bin of the whole pulses besides energy flux. Similar to Peng et al. (2009) the following data points are excluded:

(1) the resulting χ^2 per degree of freedom is -1 when fitting each time-resolved spectrum because in this case the nonlinear fitting of corresponding time-resolved spectra is failure.

(2) $\alpha < -2$ and $\beta > -2$ for the BAND model, $\alpha < -2$ for the COMP model. As Paper II pointed out that, the fitted E_{peak} represents the actual peak energy of the νF_ν spectrum only in the case of $\alpha > -2$ and $\beta < -2$ for the BAND model and $\alpha > -2$ for the COMP model.

(3) the uncertainty of its corresponding E_{peak} is larger 50% than itself. In this way, we can obtain the best statistic.

With these criterions, we can obtain useful data points of E_{peak} as well as the other parameters. At the end, we have 56 and 59 pulses for Band model and Comp model, which are denoted with sample 1 and 2, respectively.

We focus, in this study, our attentions on the decay phase of pulses. Hence the initial time of the decay phase must be determined. Similar to Peng et al. (2006, 2009) the subtract-background pulses, combining the data from the BATSE four channels are modeled with the function presented in equation (22) of Kocevski et al. (2003) because we find that this function can well describe the observed profile of a FRED pulse. In addition, a fifth parameter, t_0, which measures the offset between the start of the pulse and the trigger time, is introduced.

$$F(t) = F_m(\frac{t+t_0}{t_m+t_0})^r[\frac{d}{d+r} + \frac{r}{d+r}(\frac{t+t_0}{t_m+t_0})^{(r+1)}]^{-\frac{r+d}{r+1}}, \quad (3)$$

where t_m is the time of the pulse's maximum flux, F_m; r and d are the power-law rise and decay indexes, respectively. Note that equation (1) holds for $t \geq -t_0$, when $t < -t_0$ we take $F(t) = 0$.

To obtain an intuitive view of the result of the fit, we develop and apply an interactive IDL routine for fitting pulses in bursts, which allows the user to set and adjust the initial

pulse parameters manually before allowing the fitting routine to converge on the best-fitting model via the reduced χ^2 minimization. The fits are examined many times to ensure that they are indeed the best ones. The t_m of each pulse are found and served as the starting time of the pulse decay phase. The values, t_m, t_0 and fitting chi-square are listed in Tables 1 and 2. In this way the data points of E_p within the decay portions of the FRED pulses are extracted.

3. analysis result

3.1. the evolutionary slope seen in the FRED pluses

Since Paper I have shown that the evolutionary slope in pulse decay phase can be well modeled with a single power-law form we first adopt this form to fit the temporal evolution of E_p during the decay phase of pulse.

$$E_p(t) = \frac{E_{p,0}}{((t+t_1)/\tau)^{\delta}}, \tag{4}$$

The example plots of the fits within the decay phases are given in Figures 1 and 2, which correspond to samples 1 and 2, respectively.

In order to compare these results with the theoretical ones presented by Paper I, we also plot them in Figures 1 and 2 in a logarithmic manner for samples 1 and 2, respectively. In addition, the evolutionary slope of the fitted peak energy E_p should be $d\log E_p/d\log(t+t_0)$ rather than $d\log E_p/d\log(t+t_{trigger})$, where t_0 is the starting point of the rising segment of the FRED pulse. For each pulse of our sample we use LINFIT (Press 1992) to perform a linear least-squares fit at a 1 σ confidence level to the two quantities and have $\log E_p = W - S\log(t+t_0)$. The evolutionary slope, S, are listed in Tables 1 and 2. We first check the consistence between the power-law index δ and the slope S. Figure 3 (right panel) gives the scatter plot of them, which shows they are indeed consistent.

The distribution histogram of S is indicated in Figure 3. We find from Figure 3 for the two samples that: (i) the slopes vary from 0.23 to 1.66 for sample 1 and from 0.35 to 1.47 for sample 2; (ii) the distributions of slopes are normal and the corresponding mean values and standard deviations are around 0.73 and 0.22 for sample 1 and 0.76 and 0.22 for sample 2, respectively; (iii) the corresponding values of the medians are 0.74 and 0.76 for samples 1 and 2, respectively. These indicate that for most of the pulses the slopes are good consistent with that predicted by paper I, which showed that the evolutionary slopes of the pulse decay phase are $S_1 = 0.95 \pm 0.01$ and $S_2 = 0.75 \pm 0.01$ corresponding to the intrinsic

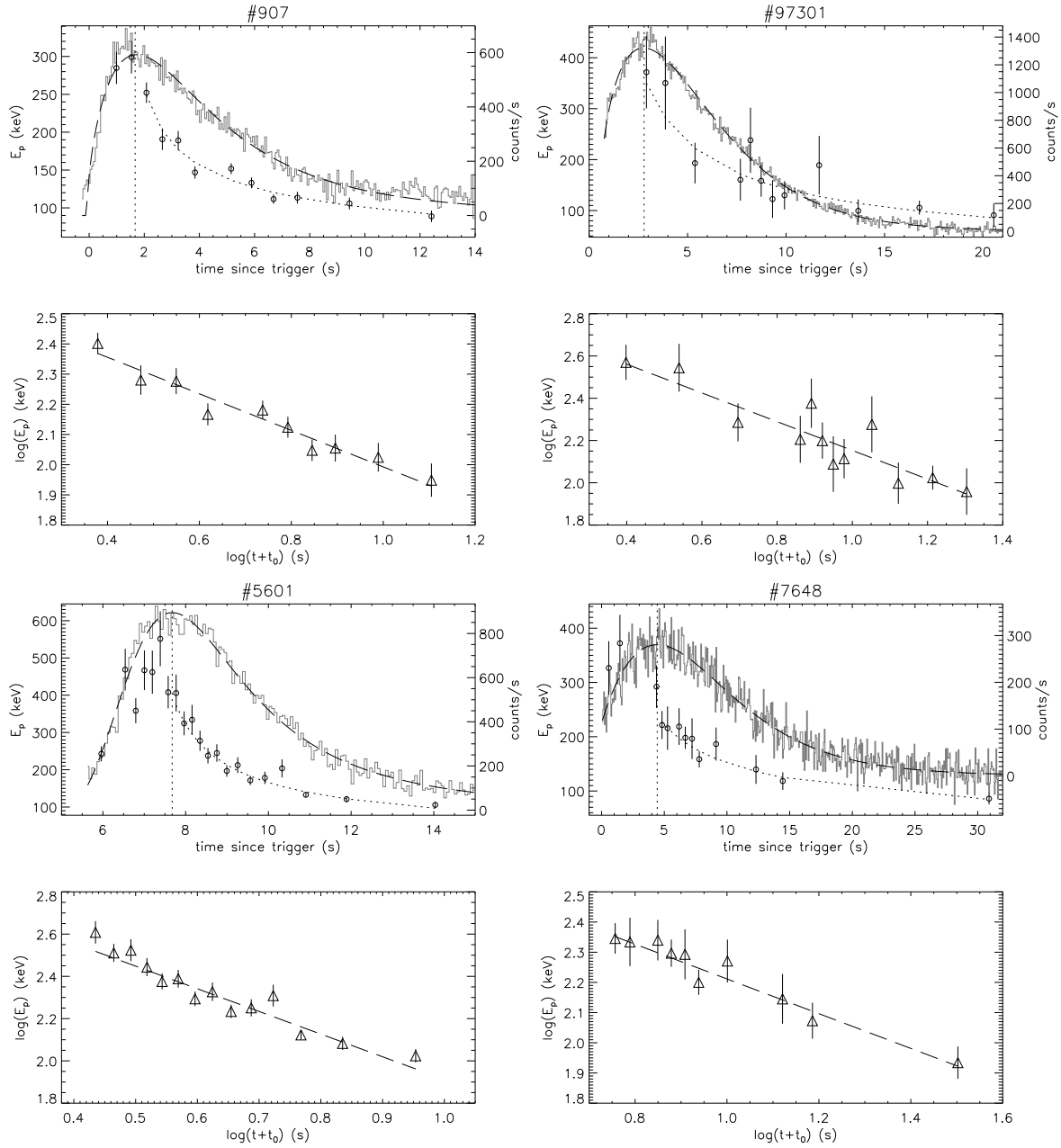

Fig. 1.— The example plots of spectral and temporal behaviors of the pulses in sample 1. The top panels show the evolutions of the peak energy E_p of the time-resolved spectra (left axes) and their corresponding pulse light curves (all four energy channels are used) (right axes). The best fit of pulse is indicated with a long dashed curve, the vertical dotted line represents the peak time of pulses, while the dotted curve is the fitting line of the E_p using a single power-law function. The bottom panel indicates the developments of the E_p within the decay phase of the pulses and the long dashed lines represent the best linear fitting.

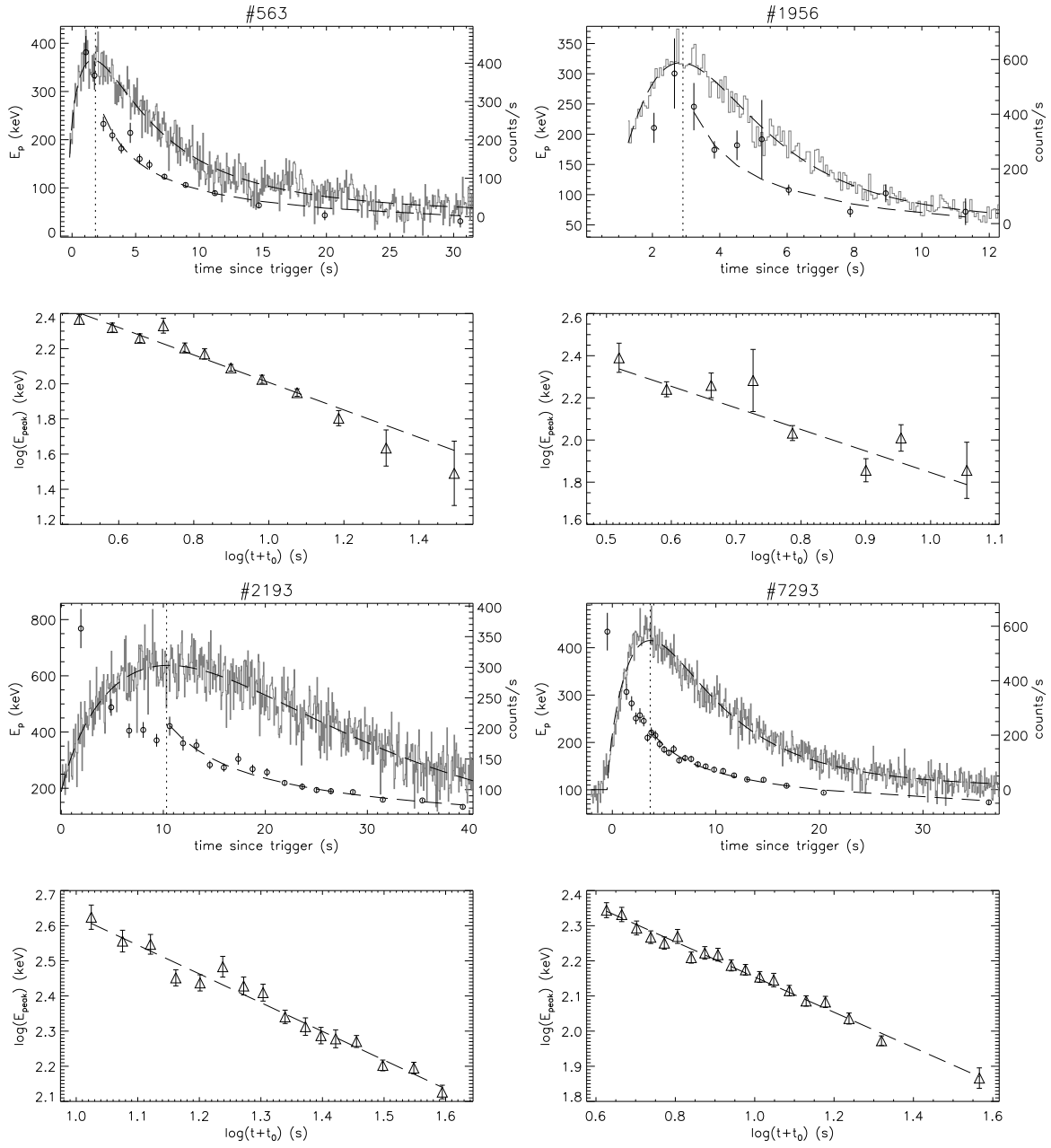

Fig. 2.— The example plots of spectral and temporal behaviors of the GRB pulses in sample 2. The meaning of the symbols are the same as figure 1.

Band function spectrum and Comptonized or thermal synchrotron spectrum, respectively. Therefore, within the limit of uncertainty the corresponding intrinsic spectra of most of bursts (about 25 for sample 1 and 29 for sample 2) may bear the intrinsic Comptonized or thermal synchrotron spectrum, whereas only a small fraction of bursts (about 16 for sample 1 and 12 for sample 2) may be associated with the intrinsic Band spectra. There are also some pulses (about 15 for sample 1 and 18 for sample 2) whose slopes are inconsistent with both theoretical values, which is similar to the result investigated by Paper I.

3.2. the relation between evolutionary slope and the spectral parameters

We suspect there is a relation between the first E_p (we denote it as $E_{p,max}$) of the decay pulse and the slope because we find that: (i) the first E_p is usually the maximal value of the decay pulse; (ii) the larger the first E_p is, the steeper of the fitting curves is. Figure 4 demonstrates the relation between $E_{p,max}$ and S for the the samples 1 (panel (a)) and 2 (panel (b)). An correlation between the two quantities is identified for both samples. For the sample 1 a liner regression analysis ($\log S = A + B \times \log E_p$) yields the intercept $A = -1.78 \pm 0.08$ and the slope $B = 0.73 \pm 0.03$, with the correlation coefficient $R = -0.67$ ($N = 56, p < 10^{-4}$). While for the sample 2, the analysis produces the intercept $A = -1.66 \pm 0.06$ and the slope $B = 0.66 \pm 0.02$, with the correlation coefficient $R = -0.68$ ($N = 59, p < 10^{-4}$).

Sakamoto et al. (2008) have showed that the E_p is correlated with the photon index (Γ) derived from a simple power-law model. Motivated by this, we also examine if there are also correlation between the E_p and the S since the S corresponds to the power-law index δ. Figure 5 displays the E_p of time-integrated spectra versus S. A clear correlated relationship between the two quantities is found. A straight line is fitted to the points: (i) $\log S = -1.16(\pm 0.032) - 0.50(\pm 0.01) \log E_p$, with the correlation coefficient $R = 0.65$ (N=56, $p < 10^{-4}$) for sample 1; (ii) $S = -1.22(\pm 0.022) - 0.51(\pm 0.01) E_p$, with the correlation coefficient $R = 0.67$ (N= 59, $p < 10^{-4}$) for sample 2.

From the Figures 4 and 5 we find that both the $E_{p,max}$ and the E_p of time-integrated spectra are correlated with the S. We deduce that there must be some relation between them. Figure 6 gives the scatter plot of the $E_{p,max}$ versus the E_p of time-integrated spectra, the corresponding correlation coefficient $R = 0.94$ (N= 56, $p < 10^{-4}$) for the sample 1 and $R = 0.92$ (N= 59, $p < 10^{-4}$) for sample 2, which indicates there are indeed strong correlation between them.

We also examine the relation between the S and lower energy index α as well as photon flux, f, (the energy range is 25-1800 keV). Figure 7 shows the plot of the α versus S. A

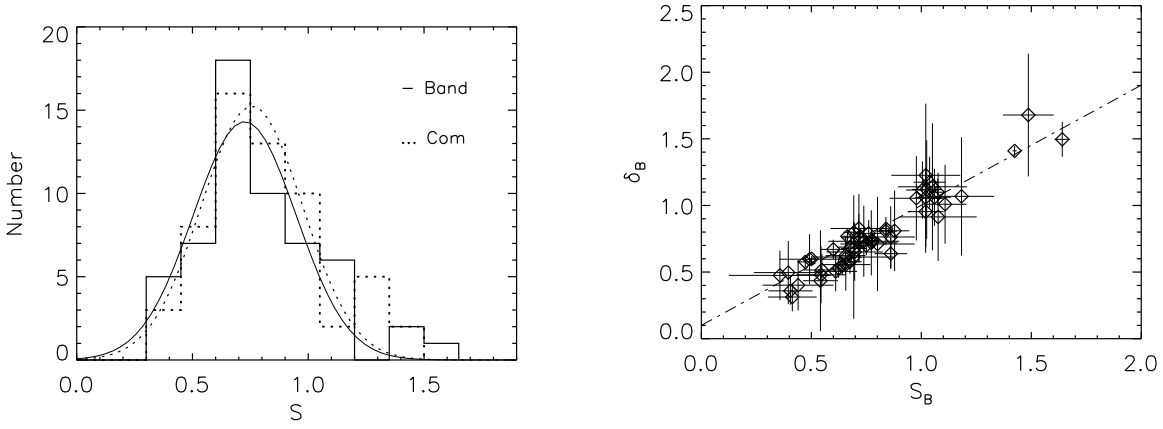

Fig. 3.— The distribution histograms of slope, S, (left panel) for sample 1 (solid line) and sample 2 (dashed line), where the curves represent the Gaussian fit to the two distributions. The right panel is the scatter plot of S vs. power-law index δ for sample 1.

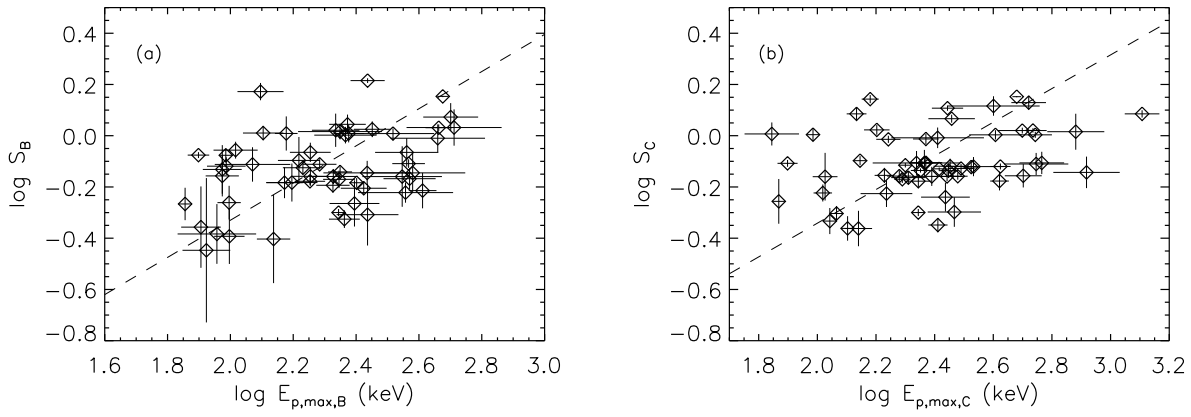

Fig. 4.— The evolutionary slope S vs. the $E_{p,max}$ of decay pulse for sample 1 (a) and sample 2 (b), where the long dashed lines represent the best fitting lines.

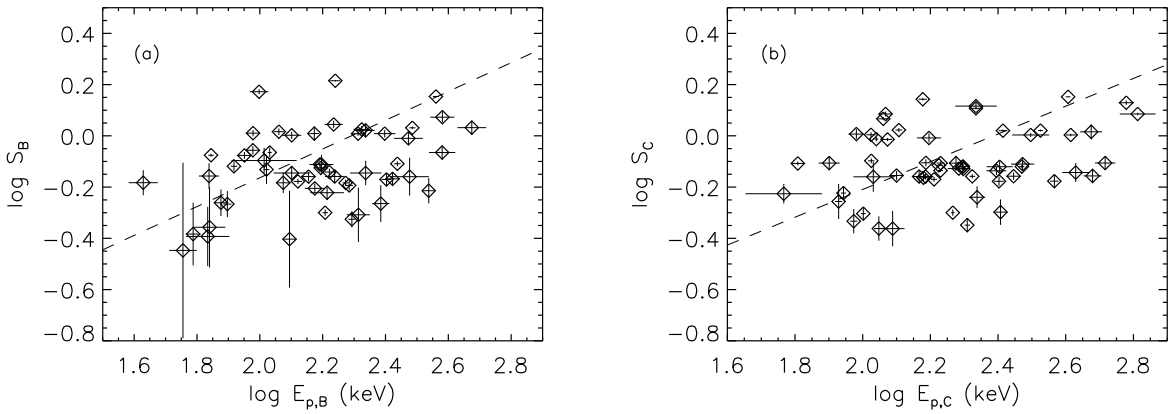

Fig. 5.— The log S vs. logE_p for sample 1 (a) and sample 2 (b).

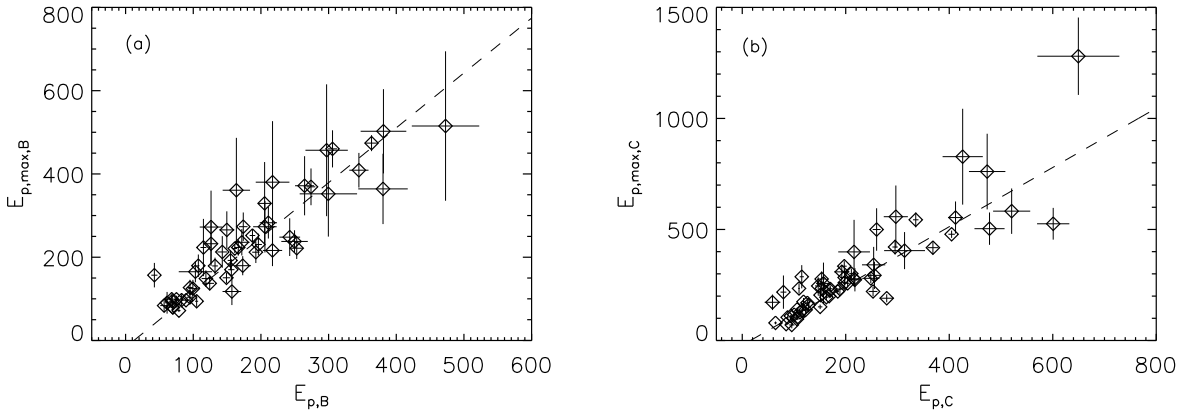

Fig. 6.— E_p of time-integrated spectra vs. the $E_{p,max}$ for sample 1 (a) and sample 2 (b). The strong correlation is indicated for both samples.

anticorrelation is suggested for both of samples with the correlation coefficient $R = -0.57$ (N= 56, $p < 10^{-4}$) for the sample 1 and $R = -0.44$ (N= 59, $p = 4.15 \times 10^{-4}$) for sample 2.

Figure 8 plots the f versus S. It is found that S is also correlated with f. The regression analysis give the best fitting line: (i) $\log S = -0.26(\pm 0.01) + 0.27(\pm 0.01) \log f$, with the correlation coefficient $R = 0.82$ (N=56, $p < 10^{-4}$) for sample 1; (ii) $\log S = -0.22(\pm 0.02) + 0.24(\pm 0.01) \log f$, with the correlation coefficient $R = 0.80$ (N= 59, $p < 10^{-4}$) for sample 2.

Since the S is related to the E_p, we wonder if there are also correlation between the S and intrinsic peak energy $E_{p,i}$. To verify the relation we need to estimate the redshifts of our selected bursts due to unknown redshift information of BATSE bursts. We attempt to use the pseudo-redshift derived by Yonetoku et al. (2004). This pseudo-redshifts were estimated based on a new relation between the spectral peak energy E_p and the 1 s peak luminosity, which was derived by combining the data of E_p and the peak luminosities by BeppoSAX and BATSE. In addition, it looks considerably tighter and more reliable than the relations suggested by the previous works (e.g. Amati et al. 2002). The intrinsic peak energy, $E_{p,i}$, in the rest frame is related with the observed E_p in the observer frame by $E_{p,i} = E_p(1 + z)$. There are 49 and 53 pulses with pseudo-redshift information in samples 1 and 2, respectively. The estimated relation between them is displayed in Figure 9.

An correlated relationship between the two quantities is also identified for both samples. The best fit functional form of this relation is $\log S = -0.923(\pm 0.047) - 0.298(\pm 0.017) \log E_{p,i}$, with the correlation coefficient $R = 0.67$ (N=50, $p < 10^{-4}$) for sample 1. For the sample 2 $\log S = -1.388(\pm 0.061) - 0.492(\pm 0.022) \log E_{p,i}$, with the correlation coefficient $R = 0.50$ (N= 53, $p < 10^{-4}$). Comparing it with the case of observed relation between S and E_p the intrinsic relation seems more loosely defined for sample 2.

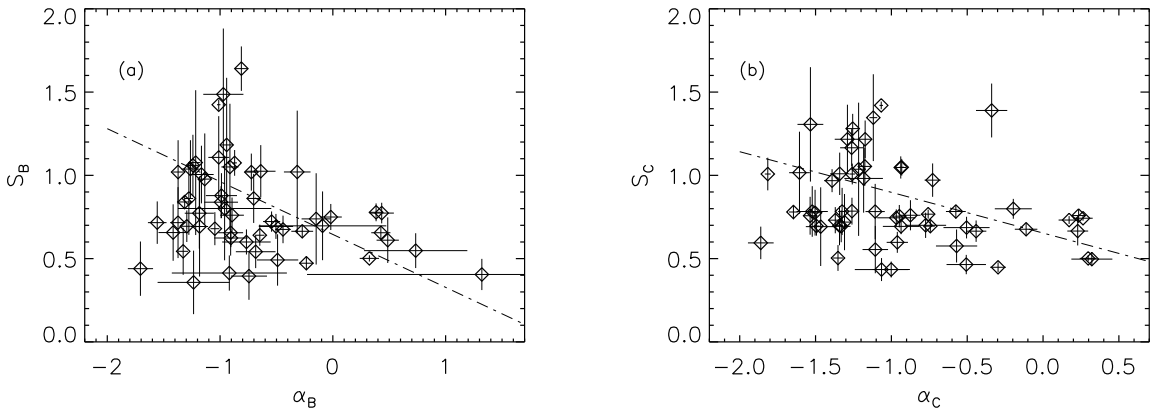

Fig. 7.— Evolutionary slope S vs. low energy index α for sample 1 (a) and sample 2 (b), where the long dashed lines represent the best fitting lines.

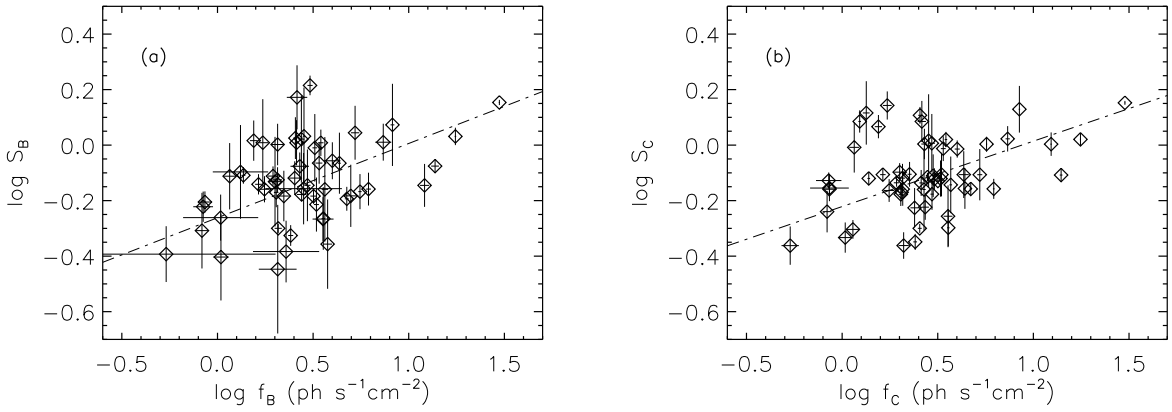

Fig. 8.— Evolutionary slope S vs. photon flux f for sample 1 (a) and sample 2 (b), where the long dashed lines represent the best fitting lines.

Table 1. A list of burst sample and various parameters for sample 1.

Trigger	F_p (phs cm^{-2}s^{-1})	time interval (s)	n	t_0 (s)	t_m (s)	$\chi^2_\nu 1$	E_p (keV)	α	δ	S	$\chi^2_\nu 2$
Band photon model											
563	1.89 ± 0.14	1.84-15.00	9	0.66 ± 0.04	1.84 ± 0.05	1.25	166.53 ± 5.74	-0.54 ± 0.07	0.77 ± 0.28	0.72 ± 0.09	1.34
907	3.57 ± 0.17	1.67-15.00	10	0.31 ± 0.04	1.67 ± 0.03	1.38	187.34 ± 4.10	0.43 ± 0.08	0.57 ± 0.07	0.66 ± 0.06	1.77
914	2.53 ± 0.16	0.61-5.00	5	1.17 ± 0.45	0.61 ± 0.02	0.92	99.46 ± 6.77	-0.97 ± 0.18	1.53 ± 0.38	1.48 ± 0.40	0.15
973_1	5.29 ± 0.20	2.79-22.00	12	-0.41 ± 0.07	2.79 ± 0.03	1.34	264.52 ± 14.11	-1.05 ± 0.04	0.68 ± 0.09	0.69 ± 0.12	0.56
973_2	5.29 ± 0.20	24.09-35.00	6	-22.14 ± 0.01	24.09 ± 0.03	1.24	217.21 ± 24.92	-1.37 ± 0.07	0.83 ± 0.24	0.72 ± 0.21	0.25
999	11.55 ± 0.31	3.99-6.00	9	-3.22 ± 0.14	3.99 ± 0.00	2.37	381.13 ± 33.72	-0.94 ± 0.05	1.05 ± 0.33	1.18 ± 0.41	0.51
1406	1.97 ± 0.13	3.35-20.00	10	0.95 ± 0.07	3.35 ± 0.05	1.07	118.71 ± 6.31	-0.91 ± 0.11	0.65 ± 0.13	0.62 ± 0.13	0.63
1883	5.20 ± 0.18	1.31-7.00	6	0.25 ± 0.07	1.31 ± 0.02	0.97	249.72 ± 19.61	-1.372 ± 0.05	0.94 ± 0.27	1.01 ± 0.20	0.56
1956	2.57 ± 0.13	2.91-15.00	8	0.07 ± 0.29	2.91 ± 0.04	1.21	126.23 ± 8.82	-1.17 ± 0.11	1.11 ± 0.14	1.00 ± 0.17	0.95
1989	2.73 ± 0.15	116.54-130.00	5	-111.58 ± 0.20	116.54 ± 0.05	1.32	89.32 ± 4.93	-0.99 ± 0.15	0.80 ± 0.05	0.84 ± 0.09	1.11
2083_1	45.42 ± 0.46	1.05-6.00	17	0.36 ± 0.22	1.04 ± 0.00	5.98	363.25 ± 8.24	-1.40 ± 0.02	1.24 ± 0.09	1.42 ± 0.03	1.15
2083_2	45.42 ±0.46	8.68-20.00	42	-4.02 ± 0.78	8.68 ± 0.01	2.26	69.95 ± 1.40	-1.31 ± 0.07	0.83 ± 0.34	0.84 ± 0.04	0.79
2138	7.00 ± 0.20	1.29-15.00	11	1.28 ± 0.21	1.29 ± 0.06	1.17	205.92 ± 17.4	-0.49 ± 0.18	0.59 ± 0.02	0.49 ± 0.15	0.58
2193	1.55 ± 0.13	10.32-42.00	15	-0.04 ± 0.5	10.32 ± 0.24	0.98	274.11 ± 6.48	0.38 ± 0.06	0.74 ± 0.46	0.78 ± 0.05	1.08
2387	3.86 ± 0.16	6.49-40.00	38	-0.53 ± 0.27	6.49 ± 0.07	1.15	132.22 ± 4.17	-0.27 ± 0.09	0.76 ± 0.04	0.66 ± 0.04	1.48
2484	1.55 ± 0.13	2.01-10.00	6	2.66 ± 0.85	2.01 ± 0.07	1.09	107.55 ± 1.60	-0.70 ± 0.06	0.67 ± 0.13	0.86 ± 0.15	0.85
2519	1.53 ± 0.14	0.59-15.00	13	0.45 ± 0.02	0.59 ± 0.06	1.02	163.76 ± 20.23	-0.77 ± 0.22	0.67 ± 0.07	0.60 ± 0.07	1.00
2662	1.52 ± 0.14	1.31-12.00	6	0.30 ± 0.05	1.31 ± 0.07	1.11	149.64 ± 11.03	-0.90 ± 0.15	0.53 ± 0.07	0.62 ± 0.09	1.15
2665	1.99 ± 0.15	1.42-8.00	7	1.22 ± 0.32	1.42 ± 0.05	0.89	105.03 ± 2.25	-0.15 ± 0.13	0.73 ± 0.22	0.74 ± 0.25	0.50
2700	4.06 ± 0.18	53.7-61.00	14	-52.84 ± 0.01	53.71 ± 0.03	1.37	242.36 ± 15.13	-1.33 ± 0.04	0.61 ± 0.21	0.54 ± 0.14	0.12
2880	2.90 ± 0.14	0.47-3.00	6	0.34 ± 0.04	0.47 ± 0.01	1.43	124.33 ± 6.46	-0.74 ± 0.16	0.46 ± 0.12	0.50 ± 0.14	0.40
2919	5.77 ± 0.19	0.34-7.00	9	1.57 ± 0.12	0.34 ± 0.02	1.39	380.43 ± 36.64	-1.28 ± 0.04	0.79 ± 0.19	0.86 ± 0.29	0.82
3003	2.83 ± 0.16	9.68-24.00	10	8.94 ± 7.15	9.68 ± 0.08	1.02	472.83 ± 49.82	-1.22 ± 0.04	0.93 ± 0.22	1.07 ± 0.73	0.40
3143	2.59 ± 0.14	0.69-4.00	8	0.64 ± 0.25	0.69 ± 0.02	0.96	99.09 ± 16.27	-0.85 ± 0.39	0.77 ± 0.44	0.80 ± 0.39	1.43
3256	1.76 ± 0.11	1.38-9.00	20	0.55 ± 0.08	1.38 ± 0.07	1.06	142.93 ± 7.39	-0.50 ± 0.15	0.65 ± 0.05	0.70 ± 0.07	0.90
3257	3.06 ± 0.13	3.51-35.00	27	0.60 ± 0.06	3.51 ± 0.06	1.10	196.33 ± 5.15	-0.24 ± 0.06	0.45 ± 0.02	0.57 ± 0.04	1.50
3290	10.71 ± 0.18	2.98-4.00	5	-2.73 ± 0.00	2.98 ± 0.01	2.52	50.84 ± 10.53	-1.69 ± 0.21	0.41 ± 0.30	0.45 ± 0.16	0.60
3415	9.16 ± 0.19	11.56-15.00	5	-10.84 ± 0.02	11.56 ± 0.01	1.44	245.74 ± 28.54	-1.21 ± 0.07	0.61 ± 0.33	0.70 ± 0.30	1.83
3648_2	5.70 ± 0.15	23.85-36.00	5	-19.47 ± 0.19	23.85 ± 0.18	0.97	75.22 ± 3.68	0.73 ± 0.45	0.52 ± 0.08	0.55 ± 0.10	1.50
3648_3	5.70 ± 0.15	41.04-48.00	12	-32.20 ± 1.44	41.04 ± 0.02	1.36	173.94 ± 6.30	-0.81 ± 0.05	1.49 ± 0.02	1.62 ± 0.09	0.85
3765	25.29 ± 0.27	66.15-73.00	12	-63.70 ± 0.24	66.15 ± 0.01	1.45	294.73 ± 7.20	-1.09 ± 0.02	1.03 ± 0.19	1.07 ± 0.08	2.05
3870	13.90 ± 0.23	0.50-6.00	9	0.46 ± 0.38	0.50 ± 0.01	1.32	118.03 ± 19.34	-1.61 ± 0.09	0.76 ± 0.06	0.72 ± 0.14	0.72

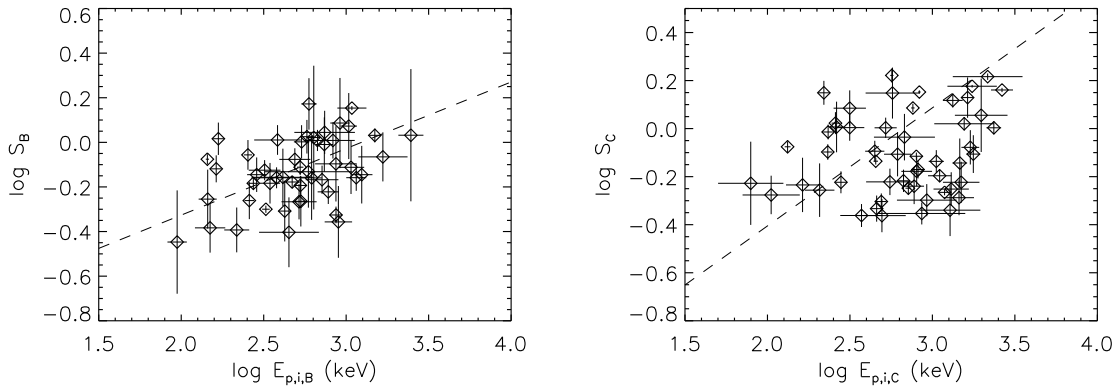

Fig. 9.— The evolutionary slope S vs. intrinsic peak energy $E_{p,i}$ for sample 1 (a) and sample 2 (b), where the long dashed lines represent the best fitting lines.

Table 1—Continued

Trigger	F_p (phs cm^{-2}s^{-1})	time interval (s)	n	t_0 (s)	t_m (s)	$\chi^2_\nu 1$	E_p (keV)	α	δ	S	$\chi^2_\nu 2$
3875	2.80 ± 0.11	0.27-3.00	8	0.14 ± 0.01	0.27 ± 0.02	1.61	69.64 ± 4.02	-1.23 ± 0.25	0.47 ± 0.21	0.36 ± 0.19	1.14
3954	8.19 ± 0.19	0.78-6.00	8	2.26 ± 1.47	0.78 ± 0.01	1.05	297.13 ±31.34	-1.14 ± 0.06	1.05 ± 0.08	0.98 ± 0.27	0.86
4350	3.27 ± 0.12	14.05-20.00	8	-13.08 ± 0.03	14.05 ± 0.04	1.49	130.96 ± 11.84	-1.55 ± 0.08	0.56 ± 0.14	0.66 ± 0.17	1.10
5478	2.96 ± 0.12	2.08-12.00	11	0.52 ± 0.05	2.08 ± 0.04	0.97	156.36 ± 4.63	-0.02 ± 0.09	0.70 ± 0.12	0.75 ± 0.08	1.58
5517	1.77 ± 0.11	0.83-6.00	9	0.18 ± 0.44	0.83 ± 0.07	0.97	157.15 ± 13.86	-1.18 ± 0.13	0.73 ± 0.21	0.77 ± 0.21	0.62
5523	3.67 ± 0.14	1.05-5.00	5	0.33 ± 0.18	1.05 ± 0.03	1.16	171.85 ± 11.44	-1.01 ± 0.09	1.01 ± 0.22	1.10 ± 0.25	0.67
5601	4.49 ± 0.14	7.67-15.00	25	-5.04 ± 0.18	7.67 ± 0.02	1.31	205.55 ±9.44	-0.72 ± 0.06	1.06 ± 0.05	1.02 ± 0.11	0.99
6159	1.94 ± 0.12	3.17-12.00	7	2.28 ± 8.25	3.17 ± 0.11	1.01	68.91 ± 5.12	-0.09 ± 0.56	0.65 ± 0.17	0.70 ± 0.21	0.89
6397	5.78 ± 0.15	3.42-25.00	13	0.55 ± 0.05	3.42 ± 0.02	1.40	192.55 ± 5.44	-0.65 ± 0.04	0.55 ± 0.06	0.64 ± 0.06	1.72
6504	2.33 ± 0.12	3.09-17.00	10	1.04 ± 0.51	3.09 ± 0.07	0.98	155.32 ± 4.29	0.43 ± 0.11	0.74 ± 0.08	0.77 ± 0.06	0.62
6621	6.71 ± 0.16	32.53-37.00	10	-29.56 ± 0.48	32.53 ± 0.02	1.09	95.04 ± 4.87	-0.98 ± 0.13	0.89 ± 0.23	0.81 ± 0.13	2.58
6625	1.81 ± 0.13	5.22-23.00	13	1.51 ± 0.84	5.22 ± 0.11	1.07	82.74 ± 1.98	-0.89 ± 0.11	0.79 ± 0.10	0.76 ± 0.11	0.86
6657	1.86 ± 0.21	4.26-47.00	5	1.31 ± 0.11	4.26 ± 0.19	1.06	70.41 ± 11.14	1.03 ± 1.38	0.36 ± 0.12	0.41 ± 0.09	0.17
6930	5.54 ± 0.18	31.83-35.00	9	-29.94 ± 0.15	31.83 ± 0.02	1.06	95.18 ± 4.34	-0.64 ± 0.13	1.12 ± 0.17	1.02 ± 0.16	0.19
7293	2.95 ±0.11	3.66-40.00	19	0.46 ± 0.05	3.66 ± 0.06	1.27	161.44 ± 3.26	0.32 ± 0.08	0.60 ± 0.02	0.50 ± 0.02	0.99
7295	3.26 ± 0.17	2.23-9.00	6	1.16 ± 0.64	2.23 ± 0.06	1.02	344.84 ± 14.25	0.49 ± 0.10	0.53 ± 0.12	0.61 ± 0.13	0.72
7475	3.69 ± 0.14	9.15-30.00	16	-0.05 ± 0.11	9.15 ± 0.05	1.84	173.14 ± 12.34	-1.29 ± 0.05	0.64 ± 0.04	0.69 ± 0.09	0.67
7548	2.95 ± 0.12	3.77-6.00	5	-1.64 ± 0.22	3.77 ± 0.03	0.98	217.14 ± 14.34	-0.91 ± 0.07	1.14 ± 0.71	1.05 ± 0.78	0.15
7588	2.08 ± 0.12	2.74-13.00	5	0.44 ± 0.27	2.74 ± 0.07	0.84	78.84 ± 2.35	-0.68 ± 0.17	0.44 ± 0.08	0.54 ± 0.10	0.34
7638	1.75 ± 0.11	1.10-9.00	16	0.92 ± 0.63	1.10 ± 0.05	1.47	61.34 ± 3.23	-0.92 ± 0.51	0.32 ± 0.11	0.41 ± 0.11	0.34
7648	1.55 ± 0.10	4.43-31.00	10	0.89 ± 0.46	4.43 ± 0.14	1.02	252.93 ± 9.04	-0.44 ± 0.06	0.58 ± 0.08	0.57 ± 0.08	0.40
7711	3.66 ± 0.13	1.98-8.00	10	2.01 ± 1.78	1.98 ± 0.04	1.28	211.03 ± 12.83	-1.24 ± 0.05	1.06 ± 0.19	1.05 ± 0.18	0.98
8049_1	1.59 ± 0.09	8.03-20.00	7	15.45 ± 9.02	8.03 ± 0.16	1.02	149.13 ± 5.45	-0.32 ± 0.11	1.21 ± 0.55	1.02 ± 0.57	0.37
8049_2	1.59 ± 0.09	30.99-80.00	9	13.15 ± 10.17	30.99 ± 0.18	0.96	115.03 ± 4.38	-1.26 ± 0.08	1.17 ± 0.15	1.04 ± 0.17	1.68

Note. — F_p denotes the peak flux on a 256 ms timescale; time interval is the interval of start and end time of decay phase of selected pulses. $\chi^2_\nu 1$ and $\chi^2_\nu 2$ are the fitting χ^2_ν of pulse light curves and the power-law decay of E_p, respectively.

Table 2. A list of burst sample and various parameters for sample 2.

Trigger	F_p (phs cm^{-2}s^{-1})	time interval (s)	n	t_0 (s)	t_m (s)	χ^2_ν1	E_p (keV)	α	δ	S	χ^2_ν2
Band photon model											
563	1.89 ± 0.14	1.84-32.00	12	0.66 ± 0.04	1.84 ± 0.05	1.25	169.53 ± 4.74	-0.58 ± 0.07	0.75 ± 0.04	0.78 ± 0.09	1.62
907	3.57 ± 0.17	1.67-16.00	16	0.31 ± 0.04	1.67 ± 0.03	1.38	198.34 ± 3.30	0.26 ± 0.06	0.67 ± 0.02	0.74 ± 0.01	1.61
914	2.53 ± 0.16	0.61-5.00	6	1.17 ± 0.45	0.61± 0.02	0.92	116.46 ± 4.77	-1.29 ± 0.08	1.20 ± 0.21	1.21 ± 0.20	1.25
973_1	5.29 ± 0.20	2.79-22.00	21	-0.41 ± 0.07	2.79 ± 0.03	1.34	412.52 ± 14.11	-1.26 ± 0.02	0.95 ± 0.09	1.00 ± 0.06	1.41
973_2	5.29 ± 0.20	24.09-35.00	7	-22.14 ± 0.01	24.09 ± 0.03	1.24	296.21 ± 24.92	-1.51 ± 0.04	0.82 ± 0.15	0.78 ± 0.14	1.25
999	11.55 ± 0.31	3.99-6.00	13	-3.22 ± 0.14	3.99 ± 0.00	2.37	600.93 ± 31.72	-1.12 ± 0.03	1.31 ± 0.31	1.34 ± 0.26	0.98
1406	1.97 ± 0.13	3.35-37.00	14	0.95 ± 0.07	3.35 ± 0.05	1.07	153.71 ± 4.84	-1.26 ± 0.05	0.79 ± 0.09	0.81 ± 0.08	0.78
1467	2.26 ± 0.13	4.47-28.00	5	0.69 ± 0.52	4.47 ± 0.04	0.99	111.64 ± 3.73	-1.01 ± 0.12	0.41 ± 0.04	0.44 ± 0.04	1.81
1733	3.00 ± 0.15	3.46-30.00	5	6.26 ± 3.25	3.46 ± 0.04	1.41	649.54 ± 79.23	-1.17 ± 0.04	1.56 ± 0.34	1.21 ± 0.17	1.66
1883	5.20 ± 0.18	1.31-12.00	7	0.25 ± 0.07	1.31 ± 0.02	0.97	248.32 ± 16.72	-1.37 ± 0.04	0.68 ± 0.17	0.74 ± 0.15	1.56
1956	2.57 ± 0.13	2.91-15.00	8	0.07 ± 0.29	2.91 ± 0.04	1.21	146.23 ± 6.24	-1.33 ± 0.06	0.76 ± 0.14	0.69 ± 0.13	1.65
1989	2.73 ± 0.15	116.54-130.00	5	-111.58 ± 0.20	116.54 ± 0.05	1.32	105.32 ± 3.29	-1.33 ± 0.06	0.93 ± 0.05	1.00 ± 0.09	1.01
2083_1	45.42 ± 0.46	1.05-6.00	17	0.36 ± 0.22	1.04 ± 0.00	5.98	404.25 ± 6.28	-1.06 ± 0.01	1.34 ± 0.09	1.41 ± 0.03	1.15
2083_2	45.42 ± 0.46	8.68-20.00	42	-4.02 ± 0.78	8.68 ± 0.01	2.26	64.31 ± 2.54	-1.64 ± 0.03	0.85 ± 0.34	0.78 ± 0.04	0.77
2138	7.00 ± 0.20	1.29-15.00	17	1.28 ± 0.21	1.29 ± 0.06	1.17	205.92 ± 17.4	-0.49 ± 0.18	0.45 ± 0.02	0.58 ± 0.15	0.58
2193	1.55 ± 0.13	10.32-42.00	15	-0.04 ± 0.5	10.32 ± 0.24	0.98	295.31 ± 15.18	0.23 ± 0.07	0.75 ± 0.06	0.96 ± 0.04	1.25
2387	3.86 ± 0.16	6.49-40.00	15	-0.53 ± 0.27	6.49 ± 0.07	1.15	167.22 ± 3.13	-0.75 ± 0.04	0.75 ± 0.03	0.77 ± 0.03	2.48
2484	1.55 ± 0.13	2.01-30.00	8	2.66 ± 0.85	2.01 ± 0.07	1.09	106.55 ± 1.65	-0.72 ± 0.03	1.05 ± 0.13	0.97 ± 0.11	0.99
2519	1.53 ± 0.14	0.59-15.00	7	0.45 ± 0.02	0.59 ± 0.06	1.02	192.76 ± 14.73	-0.97 ± 0.12	0.75 ± 0.07	0.75 ± 0.07	1.00
2662	1.52 ± 0.14	1.31-12.00	6	0.30 ± 0.05	1.31 ± 0.07	1.11	153.14 ± 7.99	-0.93 ± 0.12	0.67 ± 0.07	0.69 ± 0.07	1.45
2665	1.99 ± 0.15	1.42-8.00	8	1.22 ± 0.32	1.42 ± 0.05	0.89	106.03 ± 2.24	-0.19 ± 0.11	0.75 ± 0.12	0.79 ± 0.25	1.21
2700	4.06 ± 0.18	53.7-61.00	19	-52.84 ± 0.01	53.71 ± 0.03	1.37	255.36 ± 11.13	-1.35 ± 0.03	0.45 ± 0.21	0.50 ± 0.14	0.42
2880	2.90 ± 0.14	0.47-3.00	6	0.34 ± 0.04	0.47 ± 0.01	1.43	125.93 ± 5.46	-0.77 ± 0.14	0.76 ± 0.12	0.70 ± 0.14	1.10
2919	5.77 ± 0.19	0.34-7.00	17	1.57 ± 0.12	0.34 ± 0.02	1.39	477.43 ± 26.64	-1.34 ± 0.04	0.70 ± 0.11	0.69 ± 0.11	0.62
3003	2.83 ± 0.16	9.68-24.00	17	8.94 ± 7.15	9.68 ± 0.08	1.02	473.83 ± 39.82	-1.22 ± 0.04	0.85 ± 0.06	1.03 ± 0.43	1.20
3143	2.59 ± 0.14	0.69-4.00	6	0.64 ± 0.25	0.69 ± 0.02	0.96	216.09 ± 30.27	-1.53 ± 0.09	1.34 ± 0.44	1.30 ± 0.43	1.03
3256	1.76 ± 0.11	1.38-9.00	27	0.55 ± 0.08	1.38 ± 0.07	1.06	151.93 ± 5.39	-0.50 ± 0.15	0.65 ± 0.05	0.68 ± 0.06	0.91
3257	3.06 ± 0.13	3.51-35.00	29	0.60 ± 0.06	3.51 ± 0.06	1.10	203.33 ± 5.26	-0.31 ± 0.05	0.45 ± 0.02	0.45 ± 0.03	2.05
3290	10.71 ± 0.18	2.98-4.00	5	-2.73 ± 0.00	2.98 ± 0.01	2.52	38.45 ± 13.53	-1.86 ± 0.87	0.72 ± 0.30	0.69 ± 0.26	1.19
3415	9.16 ± 0.19	11.56-15.00	6	-10.84 ± 0.02	11.56 ± 0.01	1.44	426.74 ± 30.54	-1.31 ± 0.04	0.75 ± 0.23	0.72 ± 0.19	1.78
3648_1	5.70 ± 0.15	2.72-14.00	8	2.05 ± 0.00	2.72 ± 0.15	0.81	100.22 ± 1.68	0.32 ± 0.15	0.49 ± 0.04	0.50 ± 0.03	0.74
3648_2	5.70 ± 0.15	23.85-36.00	6	-19.47 ± 0.19	23.85 ± 0.18	0.97	94.09 ± 2.28	-0.51 ± 0.15	0.48 ± 0.06	0.46 ± 0.05	1.16

4. conclusions and discussions

Pulses are the basic, central building blocks of GRB prompt emission, and it is essential to our understanding of GRB physics (Hakkila et al. 2008). In this paper we select a well-separated single pulses presented by Kocevski et al. (2003) and Norris et al. (1999) including bright and weak bursts to investigate the evolutionary slope of E_p during the pulse decay phase. We first fit the E_p of time-resolved spectra for our selected pulses with a single power-law function form and obtain the evolutionary slope to compare it with the theoretical predication of Paper I. Our results show that these observed evolutionary slopes are in good agreement with the predictions of Paper I. Contrary to Paper I, however, we find that within the limits of uncertainty the corresponding intrinsic spectra of most of bursts (about 25 for sample 1 and 29 for sample 2) may bear the intrinsic Comptonized or thermal synchrotron spectrum, whereas only a small number of bursts (about 16 for sample 1 and 12 for sample 2) may be associated with the intrinsic Band function spectra. Paper I investigated 12 pulses and found that there are eight consisting with intrinsic Band spectrum and only two corresponding to the intrinsic Comptonized or thermal synchrotron spectrum. We argue our analysis results are more reliable for the following reasons. Firstly, the quantity of our sample (56 for Band model and 59 for Compton model) much larger than that of Paper I. Secondly, we remove all possible improperly-measured E_p, i.e. the E_p with $\alpha < -2$ and $\beta > -2$ for the BAND model, $\alpha < -2$ for the COMP model are discarded, but Paper I does not seem to consider it. Lastly, the E_p with its error larger than 50 percent of itself are also excluded but Paper I includes the E_p with much larger error. Since the Paper I pointed out that the evolutionary curve of the decay portion of the pulse is dominated by the curvature effect our results also indicate that most of the FRED pulses we selected indeed result from this effect.

There are also some outliers (about 15 for sample 1 and 18 for sample 2) included in our sample. Besides the curvature effect, there might be some other factors that can affect the value of S. One factor would be the variation of the rest-frame emission mechanism, which was revealed in Qin et al. (2005). For example, different rest-frame spectra or different speeds of the rest-frame spectral softening could lead to different values of the power-law index. Other factors pointed out by Paper I, such as the real intrinsic radiation mechanism may be more complicated as well as GRBs might be associated with more complicated situations rather than a simple fireball expanding isotropically with a constant Lorentz factor. There are some disparate E_p values that could be the result of source confusion (pulse overlapping) in the pulse decay phase (e.g. we can see from Figures 1 and 2). Maybe this is also one of the reasons giving arise to the outliers.

We also study the possible correlations between the S and other parameters. A strong

Table 2—Continued

Trigger	F_p (phs cm^{-2}s^{-1})	time interval (s)	n	t_0 (s)	t_m (s)	$\chi^2_\nu 1$	E_p (keV)	α	δ	S	$\chi^2_\nu 2$
3648_3	5.70 ± 0.15	41.04-48.00	12	-32.20 ± 1.44	41.04 ± 0.02	1.36	197.94 ± 4.30	-0.95 ± 0.05	0.69 ± 0.02	0.75 ± 0.09	1.85
3765	25.29 ± 0.27	66.15-73.00	12	-63.70 ± 0.24	66.15 ± 0.01	1.45	335.73 ± 2.94	-0.93 ± 0.15	1.05 ± 0.19	1.04 ± 0.05	0.77
3870	13.90 ± 0.23	0.50-6.00	21	0.46 ± 0.38	0.50 ± 0.01	1.32	313.03 ± 39.34	-1.82 ± 0.02	1.08 ± 0.11	1.00 ± 0.10	1.16
3954	8.19 ± 0.19	0.78-9.00	8	2.26 ± 1.47	0.78 ± 0.01	1.05	520.15 ± 35.34	-1.3 ± 0.03	0.77 ± 0.13	0.78 ± 0.14	1.41
4350	3.27 ± 0.12	14.05-20.00	10	-13.08 ± 0.03	14.05 ± 0.04	1.49	79.96 ± 11.84	-1.55 ± 0.12	0.69 ± 0.14	0.78 ± 0.17	0.45
5478	2.96 ± 0.12	2.08-12.00	20	0.52 ± 0.05	2.08 ± 0.04	0.97	162.36 ± 3.63	-0.11 ± 0.08	0.63 ± 0.12	0.67 ± 0.08	1.48
5517	1.77 ± 0.11	0.83-6.00	12	0.18 ± 0.44	0.83 ± 0.07	0.97	157.15 ± 12.86	-1.18 ± 0.13	0.97 ± 0.21	0.98 ± 0.21	0.85
5523	3.67 ± 0.14	1.05-5.00	5	0.33 ± 0.18	1.05 ± 0.03	1.16	188.85 ± 12.44	-1.11 ± 0.06	0.73 ± 0.12	0.78 ± 0.25	0.35
5601	4.49 ± 0.14	7.67-15.00	14	-5.04 ± 0.18	7.67 ± 0.02	1.31	259.55 ± 7.44	-0.94 ± 0.03	0.95 ± 0.05	1.04 ± 0.11	1.26
6159	1.94 ± 0.12	3.17-10.00	5	2.28 ± 8.25	3.17± 0.11	1.01	95.91 ± 3.12	-1.61 ± 0.06	0.94 ± 0.31	1.01 ± 0.31	0.89
6397	5.78 ± 0.15	3.42-40.00	18	0.55 ± 0.05	3.42 ± 0.02	1.40	211.55 ± 4.44	-0.75 ± 0.03	0.65 ± 0.06	0.70 ± 0.06	1.12
6504	2.33 ± 0.12	3.09-50.00	23	1.04 ± 0.51	3.09 ± 0.07	0.98	169.82 ± 4.11	-0.74 ± 0.03	0.77 ± 0.08	0.73 ± 0.06	2.12
6621	6.71 ± 0.16	32.53-37.00	11	-29.56 ± 0.48	32.53 ± 0.02	1.09	118.04 ± 3.87	-1.39 ± 0.03	0.98 ± 0.23	0.96 ± 0.13	1.41
6625	1.81 ± 0.13	5.22-25.00	21	1.51 ± 0.84	5.22 ± 0.11	1.07	87.74 ± 1.98	-1.39± 0.04	0.65 ± 0.10	0.63 ± 0.11	1.08
6657	1.86 ± 0.21	4.26-57.00	13	1.31 ± 0.11	4.26 ± 0.19	1.06	122.41 ± 9.14	-1.06 ± 0.17	0.25 ± 0.12	0.43 ± 0.09	0.97
6930	5.54 ± 0.18	31.83-35.00	9	-29.94 ± 0.15	31.83± 0.02	1.06	127.18 ± 3.34	-1.17 ± 0.04	1.07 ± 0.17	1.05 ± 0.16	1.01
7293	2.95 ± 0.11	3.66-40.00	19	0.46 ± 0.05	3.66 ± 0.06	1.27	184.44 ± 2.26	0.29 ± 0.04	0.54 ± 0.02	0.50 ± 0.02	0.94
7295	3.26 ± 0.17	2.23-9.00	7	1.16 ± 0.64	2.23 ± 0.06	1.02	368.84 ± 10.25	0.23 ± 0.06	0.52 ± 0.12	0.53 ± 0.13	2.52
7475	3.69 ± 0.14	9.15-30.00	17	-0.05± 0.11	9.15 ± 0.05	1.84	279.14 ± 10.34	-1.49 ± 0.04	0.64 ± 0.04	0.68 ± 0.09	1.56
7548	2.95 ± 0.12	3.77-20.00	7	-1.64 ± 0.22	3.77 ± 0.03	0.98	197.84 ± 14.34	-0.87 ± 0.06	0.66 ± 0.15	0.76 ± 0.08	2.15
7588	2.08 ± 0.12	2.74-13.00	5	0.44 ± 0.27	2.74 ± 0.07	0.84	84.87 ± 2.15	-1.08 ± 0.07	0.54 ± 0.08	0.55 ± 0.18	0.39
7638	1.75 ±0.11	1.10-9.00	16	0.92 ± 0.63	1.10 ± 0.05	1.47	58.44 ± 3.23	-1.86 ± 0.09	0.59 ± 0.12	0.61 ± 0.11	0.34
7648	1.55 ± 0.10	4.43-31.00	14	0.89 ± 0.46	4.43 ± 0.14	1.02	252.93 ± 8.42	-0.44 ± 0.06	0.55 ± 0.05	0.66 ± 0.06	0.58
7711	3.66 ± 0.13	1.98-8.00	23	2.01 ± 1.78	1.98 ± 0.04	1.28	216.03 ± 9.99	-1.26 ± 0.04	1.29 ± 0.09	1.28 ± 0.08	1.14
8049_1	1.59 ± 0.09	8.03-20.00	17	15.45 ± 9.02	8.03 ± 0.16	1.02	150.53 ± 5.45	-0.34 ± 0.11	1.18 ± 0.15	1.38 ± 0.16	0.92
8049_2	1.59 ± 0.09	30.99-80.00	26	13.15 ± 10.17	30.99 ± 0.18	0.96	115.03 ± 4.38	-1.26 ± 0.01	1.26 ± 0.12	1.16 ± 0.11	0.69
8111	4.21 ± 0.14	4.98-11.00	10	-4.22 ± 0.03	4.98 ± 0.02	1.17	253.93 ± 22.51	-1.54 ± 0.04	0.71 ± 0.16	0.76 ± 0.11	1.06

Note. — the meanings of the parameters are the same as table 1.

correlation between S and the $E_{p,max}$ during the phase of pulses decay is identified. There might be some important link between S and the $E_{p,max}$. Also an important correlation between the observed E_p of pulse time-integrated spectra and S exists. In order to reveal if this correlation is intrinsic we attempt to use the pseudo-redshift calculated by Yonetoku et al. (2004) to check it. We also find there is correlation between the S and intrinsic peak energy $E_{p,i}$ but for sample 2 the intrinsic correlation is looser than the observed one. One of reasons we consider is that the pseudo-redshifts may not well represent the real redshifts of our selected bursts. Another reason we suspect that the Band model may be more suitable for describing the GRB time-integrated spectra than Compton model.

E_p is one of the fundamental characteristics of the prompt emission of GRB. Based on it several important empirical relations have been proposed. One of important relations is the so-called Amati relation (Amati et al. 2002; Amati 2003), i.e. the correlation between E_p in the GRB rest frame (E_p^{src}) and the isotropic radiated energy (E^{iso}). The second correlation with much tighter correlation than Amati relation is between the E_p^{src} energy and the collimation-corrected energy (E_γ), the so-called Ghirlanda relation (Ghirlanda et al. 2004). Similarly Liang & Zhang (2005) found a good correlation between E_p^{src}, E^{iso}, and the achromatic break time in the afterglow light curve (t_{jet}). The third relationship is between E_p^{src} and the isotropic peak luminosity (L^{iso}), the so-called the E_p^{src}, L^{iso} (Yonetoku) relation (Yonetoku et al. 2004). If these relations are valid, they must be related to the fundamental physics of GRBs. Thus, E_p^{src} energy provides us important knowledge about the characteristics of the prompt emission of GRBs. In order to calculate the bolometric fluence which reflects the total radiated energy in the prompt emission the observed E_p is a crucial quantity. Therefore, the evolutionary slope might be a useful quantity to help us understand the physic of prompt emission since the evolutionary slope is related to the observed E_p as well as the intrinsic E_p.

The observed E_p decay is clearly related to the pulse peak lag described by Hakkila et al. (2008) and Hakkila & Cumbee (2009). Both the E_p decay and the pulse peak lag describe pulse spectral softening from different viewpoints (the E_p decay reveals spectral changes with time, while pulse peak lag examines a self-similar temporal structure at different energies). There are several interesting and pertinent repercussions of this.

Firstly, pulse evolution is not limited to the "pulse decay" phase. Although the pulse peak intensity is defined to be the time at which the decay begins, this is not the case: pulse peak lags indicate that the low-energy count rate is still increasing at the time of pulse peak intensity whereas the high-energy count rate has already started to decay. So, when does the pulse E_p decay begin if not at the time of pulse peak intensity? The evidence presented here from the plots in Figures 1 and 2 suggests that for most of pulses it probably starts

dropping at the pulse onset: the entire pulse likely represents a decay of E_p (this result has been mentioned before by various other authors, e.g. Norris et al. 1986). However, this observational result contradicts the theoretical conclusion of Lu et al. (2006), which states, "Now it is clear that, in the mechanism of the curvature effect, it is the decaying phase of a local pulse that contributes to the observed lags." Since Kocevski & Liang (2003) argued that the observed lag is the direct result of spectral evolution (the E_p decay through the four BATSE channels), something appears to be missing from the Lu et al. (2006) theoretical models, based on observations? We shall analyze it in detail in the future work. However, there are also some pulses whose spectra exhibit "tracking" (the observed spectral parameters follow the same pattern as the flux or count rate time profile) behaviors (e.g. Crider et al. 1997; Peng et al. 2009). The trigger 5601 demonstrated in Figure 1 is such a "tracking" pulse. In this case, the E_p starts dropping at around the pulse peak intensity, while the E_p rises during the pulse rise phase. In fact the Hakkila et al. (2008) and Hakkila & Cumbee (2009) results have showed that spectral and intensity evolution simply scale with the pulse duration. Short, "tracking" pulses should thus exhibit the same type of E_p decay as the longer pulses, but vary on too short a timescale for this variation to have been recognized in many studies.

Secondly, pulse evolution appears to be a defining characteristic of GRB pulses. The E_p decline correlates with a wide range of other pulse properties. Hakkila et al. (2008) showed that pulse duration is tightly correlated with pulse lag and anti-correlated with pulse peak luminosity, and it certainly appears that the same is true here (for example, the E_p decay correlates with the pulse decay time interval). Similar to what is found in this work Hakkila & Cumbee (2009) also found that pulse peak lag anti-correlates with pulse peak flux and correlates with pulse asymmetry, which reveals pulse shape seems related to the pulse decay rate. It seems to mean that pulse evolution is more than a characteristic of the pulse; it appears to DEFINE the pulse.

Lastly, pulse evolution appears to drive the evolution observed in GRB bulk emission. Most of GRBs exhibit hard-to-soft evolution, this is due to the smeared measurement of overlapping pulses, and to the fact that hard, short, luminous pulses typically occur near the beginning of a burst. Our paper demonstrates that spectral evolution exists at the even finer level of pulse evolution. The fact that pulse properties are correlated (pulse peak lag dictates pulse luminosity, duration, hardness, and asymmetry) suggests that internal pulse evolution is responsible for pulse-to-pulse variations and ultimately for the burst evolution.

In this study the pulses are limited to FRED pulses, which is based on the fact that the single pulses often been described by a fast rise and exponential decay as pointed out previously. Recently, Hakkila et al. (2008) and Hakkila & Cumbee (2009) suggested that

most pulses in long GRBs are really just variations of the same phenomenon. Therefore, our analysis results about evolutionary slope should apply to those non-FRED pulses.

5. Acknowledgments

We thank the anonymous referee for constructive suggestions. This work was supported by the Natural Science Fund for Young Scholars of Yunnan Normal University (2008Z016), National Natural Science Foundation of China (No. 10778726), the Natural Science Fund of Yunnan Province (2006A0027M).

REFERENCES

Amati, L., et al. 2002, A&A, 390, 81

Amati, L., 2003, ChJAA, Vol. 3, 455

Band, D., et al. 1993, ApJ, 413, 281

Crider, A., Liang, E. P., Preece, R. D., Briggs, M. S., Pendleton, G. N., Paciesas,W. S., Band, D. L., & Matteson, J. L. 1999, ApJ, 519, 206

Daigne, F., & Mochkovitch, R., 2003, MNRAS, 342, 587

Firmani, C.; Cabrera, J. I., Avila-Reese, V., Ghisellini, G., Ghirlanda, G., Nava, L., Bosnjak, Z. 2008, arXiv0811.1578

Fishman, G. J., Meegan, C. A., Wilson, R. B., et al., 1989 , BAAS, 21, 860

Fishman, G. J., et al. 1994, ApJS, 92, 229

Ford, L. A., et al. 1995, ApJ, 439, 307

Gehrels, N.; Chipman, E.; Kniffen, D. 1994, ApJS, 92, 351

Ghirlanda, G., Ghisellini, G., Lazzati, D. 2004, ApJ, 616, 331

Golenetskii, S. V., Mazets, E. P., Aptekar, R. L., Ilinskii, V.N. 1983, Nature, 306, 451.

Hailey, C. J., Harrison, F. A., Mori, K. 1999, 529, L25

Hakkila, J., Giblin, T. W., Norris, J. P., Fragile, P. C., Bonnell, J. T. 2008, ApJ, 677, L81

Hakkila, J., & Cumbee, R. S. 2009, arXiv: 0901.3171

kaneko, Y., et al. 2006, ApJS, 166, 298 (Paper II)

Kocevski, D., & Liang, E. 2003, ApJ, 594, 385

Kocevski, D., Ryde, F., and Liang, E. 2003, ApJ, 596, 389

Liang, E. P., & Kargatis, V. E. 1996, Nature, 381, 495

Liang, E., & Zhang, B. ApJ, 633, 611

Lu, R. J., Peng, Z. Y., & Dong, W., 2007, ApJ, 663, 1110 (Paper I)

Lu, R. J., Qin, Y. P., Zhang, Z. B., & Yi, T. F. 2006, MNRAS, 367, 275

Meszaros, P., & Rees, M. J. 1998, ApJ, 502, L105

Mallozzi, R. S., Preece, R. D., & Briggs, M. S. 2005, RMFIT, A Lightcurve and Spectral Analysis Tool, (Huntsville: Univ. Alabama)

Norris, J. P., Share, G. H., Messina, D. C., et al., 1986, ApJ, 301, 213

Norris, J. P., et al. 1996, ApJ, 459, 393

Norris, J. P. et al. 2005, ApJ, 627, 324

Pendleton, G. N., et al. 1997, ApJ, 489, 175

Peng, Z. Y., et al. 2006, MNRAS, 368, 1351

Peng, Z. Y., et al. 2007, ChjAA, 7, 428

Peng, Z. Y., et al. 2009, NewA, 14, 311

Preece, R. D., Pendleton, G. N., Briggs, M. S., et al. 1998, ApJ, 496, 849

Press, W. H., Teukolsky, S. A., Vetterling, W. T., & Flannery, B. P. 1992, Numerical Recipes in Fortran (2d ed. ; Cambridge: Cambridge Univ. Press)

Ryde, F. 1999, ASPC, 190, 103

Ryde, F., & Svensson, R. 2000, ApJ, 529, L13

Ryde, F., & Svensson, R. 2002, ApJ, 566, 210

Qin, Y. P. 2002, A&A, 396, 705

Qin, Y. P., Zhang, Z. B., Zhang, F. W., and Cui, X. H. 2004, ApJ, 617, 439

Qin, Y. P., Dong, Y. M., Lu, R. J., Zhang, B. B., and Jia, L. W. 2005, ApJ, 632, 1008

Qin, Y. P., Su, C. Y., Fan, J. H., & Gupta, A. C. 2006, Phys. Rev. D, 74, 063005

Qin, Y. P. 2008a, ApJ, 683, 900

Qin, Y. P., Gupta, A. C., Fan, J. H., Lu, R.-J. 2008b, JCAP, 11, 004

Qin, Y. P. 2008c, arXiv: 0806.3339

Stern, B. E., & Svensson, R. 1996, ApJ, 469, L109

Yonetoku, D., Murakami,T., Nakamura, T., Yamazaki, R., Inoue,A. K., & Ioka, K. 2004, ApJ, 609, 935

Zhang, B.-B., Zhang, B., Liang, E. W., Wang, X. Y. 2009, ApJ, 690, L10